

# A COMPREHENSIVE STUDY OF RELATIVISTIC GRAVITY USING PSR B1534+12

EMMANUEL FONSECA

Department of Physics and Astronomy, The University of British Columbia, Vancouver, BC V6T-1Z1, Canada

INGRID H. STAIRS

Department of Physics and Astronomy, The University of British Columbia, Vancouver, BC V6T-1Z1, Canada

AND

STEPHEN E. THORSETT

Department of Physics, Willamette University, Salem, OR 97301, USA

*Draft version February 26, 2014*

## ABSTRACT

We present updated analyses of pulse profiles and their arrival-times from PSR B1534+12, a 37.9-ms radio pulsar in orbit with another neutron star. A high-precision timing model is derived from twenty-two years of timing data, and accounts for all astrophysical processes that systematically affect pulse arrival-times. Five “post-Keplerian” parameters are measured that represent relativistic corrections to the standard Keplerian quantities of the pulsar’s binary orbit. These relativistic parameters are then used to test general relativity by comparing the measurements with their predicted values. We conclude that relativity theory is confirmed to within 0.34% of its predictions. Furthermore, we derive the following astrophysical results from our timing analysis: a distance of  $d_{GR} = 1.041 \pm 0.011$  kpc to the pulsar-binary system, by relating the “excess” orbital decay to Galactic parameters; evidence for pulse “jitter” in PSR B1534+12 due to short-term magnetospheric activity; and evolution in pulse-dispersion properties. As a secondary study, we also present several analyses on pulse-structure evolution and its connection to relativistic precession of the pulsar’s spin axis. The precession-rate measurement yields a value of  $\Omega_1^{\text{spin}} = 0.59^{+0.10}_{-0.11}$  °/year (95% confidence) that is consistent with expectations, and represents an additional test of relativistic gravity.

*Subject headings:* binary: close – gravitation – ISM: evolution – pulsars: individual (PSR B1534+12) – stars: distances

## 1. INTRODUCTION

Pulsars in relativistic binary systems have provided the most rigorous tests of gravitational theory in strong fields to date. High-precision timing of such an object produces a timing model that describes “post-Keplerian” (PK) effects that characterize relativistic corrections to the standard orbital elements (Damour & Deruelle 1985, 1986), as well as its nominal spin, astrometric, and environmental properties. Comparisons between measured and expected PK parameters produce tests of the gravitational theory in question. The “Hulse-Taylor” pulsar (Hulse & Taylor 1975) provided the first such positive case for general relativity, and still serves as an excellent laboratory for strong-field gravity (Weisberg et al. 2010). The recent discovery of a massive pulsar in a highly relativistic orbit with a white dwarf yields a testing ground for tensor-scalar extensions of gravitational theory (Antoniadis et al. 2013). An extensive analysis of the “double-pulsar” system (Burgay et al. 2003) constrains general relativity to within 0.05% of its predictions and remains the most stringent pulsar-timing test so far (Kramer et al. 2006).

PSR B1534+12 was discovered by Wolszczan (1991) to be in a highly inclined, 10.1-hour binary orbit with another neutron star. Follow-up timing studies on

this pulsar (Stairs et al. 1998, 2002) produced a timing solution that yielded measurements of five PK parameters:  $\dot{P}_b$ , the orbital decay of the binary system;  $\dot{\omega}$ , the advance of periastron longitude;  $\gamma$ , the time-averaged gravitational-redshift and time-dilation parameter;  $r$  and  $s$ , the “range” and “shape” of the Shapiro time delay. Simultaneous measurement of these parameters produced a self-consistent set of tests that complemented the Hulse-Taylor results by including tests based only on quasi-stationary, non-radiative PK parameters (Taylor et al. 1992). Additional results were derived using the fitted timing model, including a precise estimate of the pulsar’s distance using the measured excess of orbital decay due to relative motion (Bell & Bailes 1996). This measurement affected earlier predictions for the event rates expected for ground-based laser interferometric gravitational-wave detectors.

The time-averaged pulse profile of PSR B1534+12 is undergoing a secular change in observed radiation pattern at a rate of 1% per year (Arzoumanian 1995). Such changes can be linked to spin-orbit coupling in a strong gravitational field, which results in a precession of the pulsar’s spin axis (“relativistic spin precession”; de Sitter 1916) and an evolving view of the two-dimensional beam structure (Kramer 1998). Stairs, Thorsett, & Arzoumanian (2004) (hereafter STA04) developed a general technique to characterize the overall profile shape at a given epoch and derive a precession rate by measuring and comparing spin-precession and orbital-aberration

efonseca@phas.ubc.ca  
 stairs@astro.ubc.ca  
 thorsett@willamette.edu

TABLE 1  
TIMING PARAMETERS FOR EACH BACKEND AND FREQUENCY

Parameter	Mark III	Mark IV	Mark IV	ASP	ASP	ASP	ASP	ASP
Frequency (MHz) ..	1400	430	1400	424	428	432	436	1400
Bandwidth (MHz) .	40	5	5	64	64	64	64	64
Spectral Channels ..	32	1 <sup>a</sup>	1 <sup>b</sup>	1	1	1	1	16 <sup>c</sup>
Number of TOAs ..	1185	3102	664	1204	1197	1190	1124	231
Dedispersion type .	Incoh.	Coh.	Coh.	Coh.	Coh.	Coh.	Coh.	Coh.
Integration time (s)	300	190	190	180	180	180	180	180
Date span (years) .	1990-94	1998-2005	1998-2005	2004-12	2004-12	2004-12	2004-12	2004-12
RMS residual, $\sigma_{rms}$	5.31	4.21	6.73	4.48	4.34	4.65	4.93	8.27

<sup>a</sup> Four sub-bands centered at 430 MHz were taken when the Mark IV data were originally recorded, but were averaged together to build signal strength.

<sup>b</sup> Two sub-bands centered at 1400 MHz were taken when the Mark IV data were originally recorded, but were also averaged together to build signal strength.

<sup>c</sup> The number of actual channels recorded sometimes varied due to computational limitations, so this value represents a typical number of channels used.

effects that produce the observed shape evolution. The results of this study yielded a direct measurement of the precession rate that was consistent with the rate predicted by general relativity, albeit with considerably limited precision. Relativistic spin precession was detected in the double-pulsar system as well, but was measured by modeling a time-dependent flux decrement during eclipses due to a precessing magnetic field (Breton et al. 2008). Furthermore, the geometry of PSR B1534+12 and its binary system was derived by combining these results with a rotating-vector-model (RVM, Radhakrishnan & Cooke 1969) analysis of the evolving polarization properties. PSR B1534+12 currently remains the only pulsar for which special-relativistic orbital aberration is observed.

In this work, we report on updated timing and profile-evolution analyses of PSR B1534+12, using data sets that collectively span 22 years since its discovery. Results from the analyses described below include improvements in tests of general relativity, an improved measurement of the pulsar’s precession rate, and additional findings extracted from our time series. A full discussion of all current results is provided in Section 5.

## 2. OBSERVATIONS AND REDUCTION

Data were obtained exclusively with the 305-m Arecibo Observatory in Puerto Rico, using two observing frequencies and three generations of pulsar signal processors. Basic information regarding the data and backends used in this analysis are presented in Table 1, while a more detailed account of observing information can be found in Fonseca (2012).

Part of this set of pulse profiles and times-of-arrival (TOAs) were recorded with the Mark III (Stinebring et al. 1992) and Mark IV (Stairs et al. 2000) pulsar backends. The Mark III system employed a brute-force pulse de-dispersion algorithm by separating each receiver’s bandpass into distinct spectral channels with a filterbank, detecting the signal within each channel, and shifting the pulse profile by the predicted amount of dispersive delay for alignment and coherent averaging. A small amount of Mark III data was obtained using the coherent-dedispersion “reticon” subsystem; these data were used only in the polarization analysis. The Mark IV machine was an instrumental upgrade which employed the now-standard coherent de-dispersion technique (Hankins & Rickett 1975) that samples and filters

the data stream prior to pulse detection. A series of digital filters applied in the frequency domain completely remove the predicted dispersion signatures while retaining even greater precision than the Mark III counterpart. See Stairs et al. (1998, 2002) for more details on these observing systems and reduction of PSR B1534+12 data obtained with these two backends.

Recent data were collected with the Arecibo Signal Processor (ASP; Demorest 2007), a further upgrade from the Mark III/IV systems that retains the coherent de-dispersion technique, but first decomposes the signals across a bandwidth of 64 MHz into a number of 4-MHz spectral channels that depends on the observing frequency. We used data collected with the four inner-most spectral channels centered on 430 MHz, and typically sixteen channels centered on 1400 MHz with some variability, due to limits in computer processing and available receiver bandpass. While the Mark IV machine used 4-bit data sampling in 5-MHz-bandpass observing mode and 2-bit sampling in 10-MHz-bandpass observing mode, ASP always used 8-bit sampling. The coherent de-dispersion filter is applied to the raw, channelized data, which are then folded modulo the topocentric pulse period within each channel and recorded to disk, preserving polarimetric information.

Observations were generally conducted at semi-regular intervals, with typical scan lengths of an hour for each frequency. Several extensive “campaign” observations were also conducted at 430 MHz, which consisted of several-hour observing sessions performed over 12 consecutive days, in order to obtain high-precision snapshots of the pulse profile at different times. Campaign sessions occurred during the summers of 1998, 1999, 2000, 2001, 2003, 2005, and 2008. We used all available data for the timing analysis, and only used most of the campaign profiles and several strong bi-monthly scans for the profile analysis. We excluded the 2008 ASP data from the profile-shape analysis due to weak, heavily scintillated signals recorded during this epoch, but used several stronger observations during this campaign for the RVM analysis (see Section 4).

We used the template cross-correlation algorithm developed by Taylor (1992) for determining pulse phases, their TOAs and uncertainties using a standard-template profile. A standard template was derived for the Mark III and Mark IV backends at each frequency by averaging

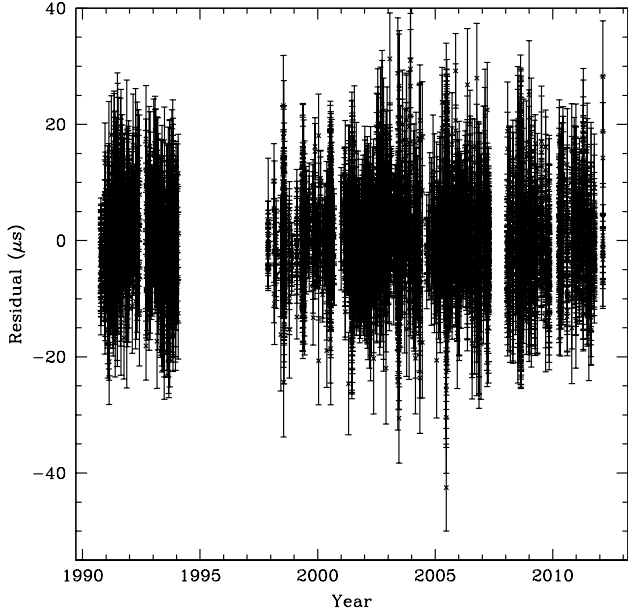


FIG. 1.— Post-fit timing residuals of PSR B1534+12. The best-fit RMS residual is  $\sigma_{\text{RMS}} = 4.57 \mu\text{s}$ .

several hours of consecutive pulse profiles; ASP TOAs were derived using the Mark IV templates. We added small amounts of error in quadrature or as factors to the original TOA uncertainties, in order to compensate for apparent systematic errors in TOAs. We also ignored TOAs with uncertainties greater than  $10 \mu\text{s}$ ; only 10% of all available TOAs – including points affected by radio frequency interference – were excised when using this cut.

It is important to note that there is a overlap in pulse TOAs collected with the Mark IV and ASP data sets between MJD 53358 and 53601. We incorporated TOAs acquired from both machines during this era, despite the overlap, due to the substantially larger ASP bandwidth; we believe that this difference in bandwidth does not produce many redundant data points. The improvement in bit sampling between backends has a measurable effect on the pulse profile shape, as discussed in Section 4 below.

### 3. TIMING ANALYSIS

Each pulse TOA was initially recorded at a local, topocentric time  $t$  and subsequently transformed to the Solar-system barycentric reference frame by accounting for a series of physical timing delays. We used the standard pulsar-analysis procedure where observed TOAs and their pulse phases are compared to the model introduced through these timing delays by using a  $\chi^2$ -minimization fitting algorithm (Lorimer & Kramer 2005). This best-fit timing solution was derived using the TEMPO pulsar-timing software package<sup>1</sup>, along with the JPL DE414 planetary ephemeris.<sup>2</sup> Fitted spin, astrometric, and DM parameters are shown in Table 2 with respect to the quoted reference epoch.

<sup>1</sup> <http://tempo.sourceforge.net>

<sup>2</sup> <http://naif.jpl.nasa.gov/naif/>

The increased timespan and updated planetary ephemeris permitted the significant measurement of a second and third time-derivative in spin frequency. Due to overlap in data between the Mark IV and ASP machines, we first fitted for an offset between these two multi-frequency sets using only 430-MHz data during this timespan while holding all model parameters fixed. We then held this offset fixed while fitting for an additional offset between the Mark III and “combined” Mark IV and ASP data during the global fit.

Moreover, we modeled the pulsar’s DM in five contiguous bins due to observed evolution in electronic content along the line of sight to PSR B1534+12. An offset from a nominal DM value and a time-derivative were determined within each bin during the global fit. We used and fixed the Mark III DM bin derived by Stairs et al. (1998) due to systematic errors they found in the Mark III 430 MHz TOAs, which we discarded from this study. The results of this DM fitting are displayed in Figure 2. The data points and their error bars in Figure 2 were determined by fixing all newly-determined parameters and fitting for DM in smaller bins of 80 days in width, without time-derivatives. We ultimately used the large-bin method during the global fit in order to minimize the total number of fitted parameters.

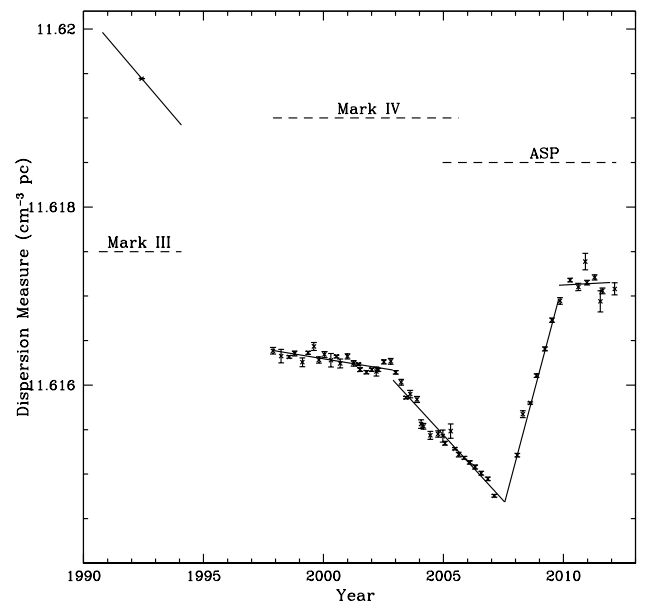


FIG. 2.— Dispersion measure (DM) of PSR B1534+12 versus time. The solid lines represent time-derivatives that were fixed or fitted when generating the global timing solution (see text). Data points and their error bars demonstrate DM fitting over smaller intervals in time.

In order to extract relativistic information about this system, we first used the “Damour-Deruelle” (DD) binary prescription (Damour & Deruelle 1986) that measures PK parameters in a phenomenological manner during the global fit. We then used the “DDGR” model, which assumes that general relativity is correct and relates each PK parameter to one or both of the binary-component masses (e.g. Stairs et al. 1998), in order to

TABLE 2  
FITTED ASTROMETRIC, SPIN AND DM PARAMETERS

Parameter	Value
Right Ascension, $\alpha_{J2000}$ .....	15 <sup>h</sup> 37 <sup>m</sup> 09 <sup>s</sup> .961724(6)
Declination, $\delta_{J2000}$ .....	11°55′55″.44380(12)
Proper motion in R.A., $\mu_\alpha$ (mas yr <sup>-1</sup> ) ..	1.487(14)
Proper motion in Decl., $\mu_\delta$ (mas yr <sup>-1</sup> ) ..	-25.29(2)
Timing parallax, $\pi$ (mas) .....	0.9(4)
Parameter reference epoch (MJD) .....	52077
Rotational frequency, $\nu$ (Hz) .....	26.3821327768940(2)
First frequency derivative, $\dot{\nu}$ (10 <sup>-15</sup> Hz <sup>2</sup> )	-1.686096(4)
Second freq. derivative, $\ddot{\nu}$ (10 <sup>-29</sup> Hz <sup>3</sup> ) ..	1.7(2)
Third freq. derivative, $\dddot{\nu}$ (10 <sup>-36</sup> Hz <sup>4</sup> ) ...	-1.6(4)
Dispersion measure, DM 1 (cm <sup>-3</sup> pc) ...	11.61944(2) <sup>a</sup>
DM derivative 1 (cm <sup>-3</sup> pc yr <sup>-1</sup> ) .....	-0.000316(10) <sup>a</sup>
Bin 1 range, epoch (MJD) .....	48178-49380, 48778 <sup>a</sup>
DM 2 (cm <sup>-3</sup> pc) .....	11.61627(3)
DM 2 derivative (cm <sup>-3</sup> pc yr <sup>-1</sup> ) .....	-0.000044(17)
Bin 2 range, epoch (MJD) .....	50775-52600, 51687.5
DM 3 (cm <sup>-3</sup> pc) .....	11.61537(4)
DM 3 derivative (cm <sup>-3</sup> pc yr <sup>-1</sup> ) .....	-0.000294(14)
Bin 3 range, epoch (MJD) .....	52601-54300, 53450.5
DM 4 (cm <sup>-3</sup> pc) .....	11.61583(8)
DM 4 derivative (cm <sup>-3</sup> pc yr <sup>-1</sup> ) .....	0.00101(5)
Bin 4 range, epoch (MJD) .....	54301-55125, 54713
DM 5 (cm <sup>-3</sup> pc) .....	11.6171(2)
DM derivative 5 (cm <sup>-3</sup> pc yr <sup>-1</sup> ) .....	-0.00001(10)
Bin 5 range, epoch (MJD) .....	55126-55974, 55550

NOTE. — Values in parentheses denote the uncertainty in the preceding digit(s).

<sup>a</sup> Taken from Stairs et al. (1998) and fixed during the global fit.

determine the masses. The fitted DD and DDGR parameters are shown in Table 3.

All uncertainties for fitted timing parameters are twice the 1- $\sigma$  TEMPO value determined from the global fit. It is common practice in pulsar timing analyses to report uncertainties that are twice as large as the formal fitted errors, in order to account for unmodeled systematic contributions from pulse “jitter” (see Section 5.1 below) to TOA measurement uncertainties. Extensive experience has shown that the resulting error bars correspond closely to 68% uncertainty ranges.

#### 4. PROFILE-EVOLUTION ANALYSIS

An observed pulse produces a set of Stokes-vector pulse profiles, from which a TOA can be derived when cross-correlating the total-intensity profile  $P$  with a standard template as described in Sections 2. As with pulsar timing, strong-field effects can give rise to observable changes in pulse-structure parameters, such as pulse-profile shape and polarization properties, over a variety of timescales. In order to detect such changes, we shifted our 430-MHz profiles to a common phase using the derived DD-binary timing model described in Section 3. Each set of campaign data was then binned into twelve orbital-phase cumulative profiles, while several strong bi-monthly scans were averaged into single profiles recorded at their respective epochs. We subsequently performed two distinct analyses on these total-intensity and polar-

ization data in order to extract gravitational information from independent techniques, as described below.

For the first analysis, we employed the model developed by STA04 that establishes pulse-structure data as functions of time and location within the relativistic orbit. Values of the total-intensity profile shape  $F$  at a given epoch were derived by first applying a principal component analysis (PCA) on a set of total-intensity profiles collected over time; the first and second principal components correspond to a “reference” ( $P_0$ ) and “difference” ( $P_1$ ) profile, respectively, and are related to an observed profile within this timespan using the relation  $P = c_0 P_0 + c_1 P_1$ . The coefficients  $c_0$ ,  $c_1$  were estimated using a cross-correlation algorithm between the observed profiles and principal components in the frequency domain, and the shape  $F$  of each profile was then estimated by calculating the ratio  $F = c_1/c_0$  in order to negate epoch-dependent scintillation effects.

The shape  $F$  of a profile recorded at time  $t$  and eccentric anomaly  $u$  can also be determined using the relation

$$F = \frac{dF}{dt}t + \delta_A F(u) + \epsilon \quad (1)$$

where  $\epsilon$  is an intercept parameter and  $dF/dt$  and  $\delta_A F$  are functions of the pulsar’s precession rate  $\Omega_1^{\text{spin}}$  and the angle  $\eta$  between the line of nodes and the projection of the spin axis on the plane of the sky:

$$\frac{dF}{dt} = F' \Omega_1^{\text{spin}} \cos \eta \sin i \quad (2)$$

$$\delta_A F = F' \frac{\beta_1}{\sin i} [-\cos \eta S(u) + \cos i \sin \eta C(u)] \quad (3)$$

The parameter  $F' = dF/d\zeta$  characterizes the unknown beam structure as a function of the auxiliary “viewing” angle  $\zeta$ ,  $\beta_1 = 2\pi x/(P_b \sqrt{1 - e^2})$  is the mean orbital velocity of the pulsar, and  $C(u) = \cos[\omega + A_e(u)] + e \cos \omega$  and  $S(u) = \sin[\omega + A_e(u)] + e \sin \omega$  are time-dependent orbital terms that depend on the true anomaly  $A_e(u)$ . All binary parameters in Equations 2 and 3 were determined through pulsar-timing techniques described in Section 3. We fitted Equation 1 to our 430-MHz data using a Markov-chain Monte Carlo (MCMC) implementation with a Metropolis algorithm in order to obtain posterior distributions of  $\Omega_1^{\text{spin}}$ ,  $\eta$ ,  $F'$ , and  $\epsilon$  from uniform priors. The results of this fitting procedure are summarized in Table 4 and discussed in Section 5.4 below.

As a second analysis, we fitted an RVM to available polarization position-angle data on each full-sum campaign profile. With the assumption of a dipolar magnetic geometry, an RVM fit yields the angle between the pulsar’s spin and magnetic axes ( $\alpha$ ), as well as the minimum-impact angle between the magnetic pole and line of sight ( $\beta$ ). While no evolution is expected in  $\alpha$ , spin precession will cause  $\beta$  to evolve with time such that  $d\beta/dt = \Omega_1^{\text{spin}} \cos \eta \sin i$  (Damour & Taylor 1992). The combination of MCMC and RVM analyses therefore yields a test on observed profile evolution due to relativistic spin precession from two independent measurements.

The differences in data quality between Mark IV and ASP profiles can be seen as slight differences in the

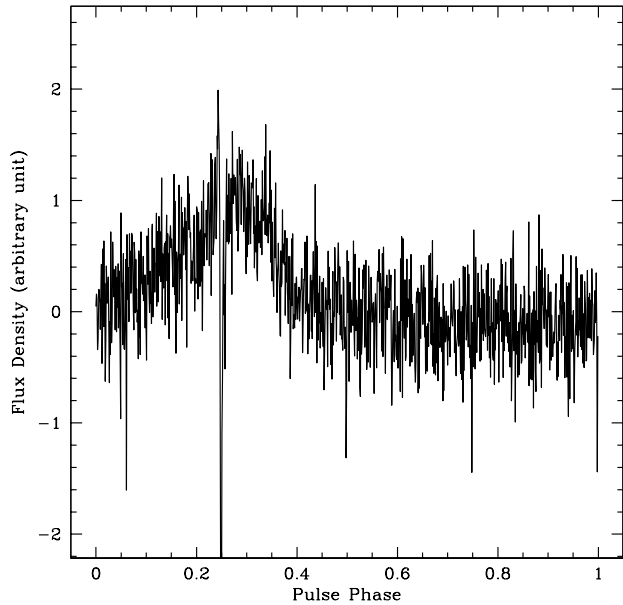


FIG. 3.— Difference between cumulative 2005 campaign profiles for the Mark IV and ASP backends.

profile shape across pulse phase, as shown in Figure 3. This introduced slight discrepancies in the PCA results when performing a full analysis using all available data, which subsequently affected the derived profile shapes and MCMC results. Two separate studies between backends were not possible as the ASP era consisted of fewer profiles and a smaller timespan, with the 2008 campaign being excluded from the MCMC analysis due to having many low signal-to-noise profiles. We therefore decided to perform a PCA on all Mark IV profiles only, and then use the derived principal components to estimate the shapes for all high signal-to-noise Mark IV and ASP profiles. This approach does not account for observed scintillation or profile evolution across frequency in ASP data, and therefore only used ASP data collected with the two innermost frequency channels centered on 430 MHz for both analyses in order to minimize such effects.

## 5. DISCUSSION

### 5.1. Pulse Jitter in PSR B1534+12

The measurability of  $\ddot{\nu}$  and  $\ddot{\nu}$  in PSR B1534+12 strongly suggests a significant amount of timing noise across our data set. This polynomial whitening in our best-fit model removes most of the long-term timing noise, which is usually attributed to rotational instabilities and variations in magnetospheric torque. However, TOA residuals generally exhibit scatter on shorter, pulse-period timescales in excess of standard measurement uncertainties. This residual “jitter” is manifested from slight changes in the shape, amplitude and pulse phase of recorded profiles between successive pulses, and is likely due to variable activity within the pulsar magnetosphere. Recent studies of pulse jitter suggest that timing precision can be improved when averaging consecutive TOA residuals together (Shannon & Cordes 2012).

We believe that such pulse jitter is evident in our timing analysis of PSR B1534+12. Figure 4 displays TOA

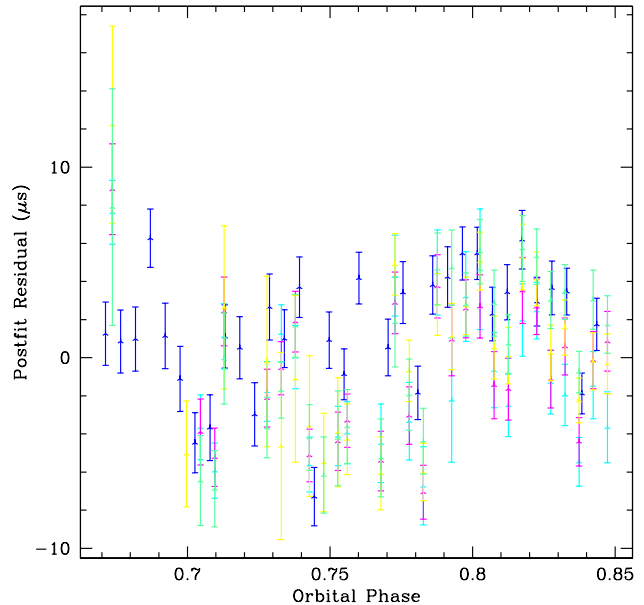


FIG. 4.— Pulse jitter in PSR B1534+12. The above figure shows global-fit residuals of TOAs recorded on MJD 53545 as a function of orbital phase. The dark-blue points were recorded with the Mark IV pulsar backend, and the remaining colors represent the four channels of ASP 430-MHz data recorded simultaneously.

residuals as a function of orbital phase from a global fit using unweighted TOA uncertainties recorded simultaneously on MJD 53545. The dark-blue data points were recorded with the Mark IV backend, while additional points represent the four channelized ASP data sets. While residual variations are visibly uncorrelated within the shown timescale, there is a visible correlation between the two overall data sets despite significant differences in backend specifications. We therefore associate this backend-correlated scatter as pulse jitter due to irregular activity within the pulsar’s magnetosphere.

Several implications arise from the observed pulse jitter. First, pulse jitter will become a significant source of timing error in future timing studies of PSR B1534+12. The recent installation of the PUPPI signal processor<sup>3</sup> is expected to produce high-precision residuals with scatter that strongly reflects time-dependent inhomogeneities in the magnetosphere. Second, a long-term solution to jitter with PSR B1534+12 cannot involve averaging a large number of consecutive TOAs. The main objective of strong-gravity tests with pulsars is to monitor time-dependent changes to orbital elements and quasi-static PK parameters, which requires full coverage of the orbit over long periods of time. We therefore use this jitter as a means to justify the TOA-uncertainty compensation for the global timing solution described in Section 2. Lastly, further instrumental upgrades will only improve measurements made at 1400 MHz, where PSR B1534+12 is intrinsically weaker and signal-to-noise is currently limited. However, the overall timing solution is still expected to improve with additional observations over time.

<sup>3</sup> <http://www.naic.edu/~astro/guide/node11.html>

TABLE 3  
ORBITAL ELEMENTS FOR PSR B1534+12

Parameter	DD Model	DDGR Model
Projected semimajor axis, $x$ (s) .....	3.7294636(11)	3.7294641(3)
Eccentricity, $e$ .....	0.27367752(14)	0.27367740(7)
Epoch of periastron, $T_0$ (MJD) .....	52076.82711326(2)	52076.827113271(19)
Orbital Period, $P_b$ (days) .....	0.420737298879(5)	0.420737298881(4)
Argument of periastron, $\omega$ (deg) .....	283.30601(2)	283.30603(2)
Rate of periastron advance, $\dot{\omega}$ (deg yr <sup>-1</sup> ) ...	1.755795(4)	1.755795 <sup>a</sup>
Time-averaged gravitational redshift, $\gamma$ (ms)	2.0707(9)	2.0701 <sup>a</sup>
Orbital decay, $(\dot{P}_b)^{\text{obs}}$ (10 <sup>-12</sup> ) .....	-0.1366(5)	-0.19244 <sup>a</sup>
Shape of Shapiro delay, $s = \sin i$ .....	0.977(3)	0.97496 <sup>a</sup>
Range of Shapiro delay, $r = T_\odot m_2$ ( $\mu$ s) ....	6.6(5)	6.627 <sup>a</sup>
Companion mass, $m_2$ ( $M_\odot$ ) .....	1.35(11)	1.3455(4)
Pulsar mass, $m_1$ ( $M_\odot$ ) .....	...	1.3330(4) <sup>a</sup>
Total mass, $M = m_1 + m_2$ ( $M_\odot$ ) .....	...	2.678463(8)
Excess $\dot{P}_b$ (10 <sup>-12</sup> ) .....	...	0.0558(5)

NOTE. — Values in parentheses denote the uncertainty in the preceding digit(s).

<sup>a</sup> derived quantity

### 5.2. Long-term Variations in Dispersion Measure

Figure 2 illustrates an irregular evolution in DM over time for PSR B1534+12. Five time-derivatives are used in our timing model to fully describe the observed changes across different timespans. Recent studies have shown that, while not as common as single-gradient variations, several objects also exhibit nonlinear evolution in DM along different directions and distances (e.g. Keith et al. 2013). As with these studies, we believe that the dominant source of such evolution is the inhomogeneity of the interstellar medium, which is traced by the pulsar’s signal as the line of sight sweeps through different regions due to a significant relative motion. These long-term timing measurements are useful for a statistical analysis of turbulence within the interstellar medium, which is usually done by calculating the spatial structure function from DM variations (e.g. You et al. 2007). Such an analysis will be presented elsewhere.

### 5.3. High-precision Distance to PSR B1534+12

Relative acceleration between the observatory and pulsar systems in the Galactic potential causes significant Doppler-factor biases in PK parameters. Stairs et al. (1998, 2002) noted such behavior in earlier data sets of PSR B1534+12 with the observed orbital decay and applied a distance-dependent kinematic correction derived by Damour & Taylor (1992) in order to include it as a consistent, radiative test of general relativity (see Section 5.5 below). However, the corrected value yielded a large uncertainty due to the imprecise distance to the pulsar derived from DM measurements using the Taylor & Cordes (1993) model of free electrons in the Galaxy. Previous studies of PSR B1534+12 therefore solved the inverse problem suggested by Bell & Bailes (1996), where general relativity is assumed to be correct; the distance is then derived using the measured “excess” orbital decay, a model of the Galactic acceleration (Kuijken & Gilmore 1989), and the expression for kinematic correction derived by Damour & Taylor (1992). Using this procedure, Stairs et al. (2002) were able to derive a distance with a relative uncertainty of 4.9%.

We used the same approach in this study to update the derived distance with a substantially longer timespan of Arecibo data. We also corrected the expression for the kinematic bias presented in Stairs et al. (1998, 2002) for missing factors of the cosine of the pulsar’s galactic latitude; the correct equation is given by Nice & Taylor (1995). Our derived distance to PSR B1534+12, using our timing results, the corrected kinematic equation and updated Galactic parameters from Reid et al. (2014), is

$$d_{\text{GR}} = 1.041 \pm 0.011 \text{ kpc} \quad (4)$$

where the value and its uncertainty (68% confidence level) were estimated using a Monte-Carlo method. This new distance is consistent with the previous estimate of  $1.02 \pm 0.05$  kpc made by Stairs et al. (2002). The relative uncertainty of this result (1.07%) is slightly lower than that of the derived distance to PSR J0437-4715 estimated by Verbiest et al. (2008). We attribute this improvement in precision to the updated  $(\dot{P}_b)^{\text{obs}}$  listed in Table 3. The uncertainty in  $d_{\text{GR}}$  is dominated by uncertainties in Galactic acceleration and rotation parameters used to derive the estimate.

Despite its high level of precision, the derived distance presented in Equation 4 is a model-dependent quantity. An ideal measure of distance can be obtained from the geometric, model-independent parallax through low-frequency interferometry. The recent inclusion of PSR B1534+12 into an extension of the PSR $\pi$  interferometry program<sup>4</sup> will likely provide such an estimate in the next 2-3 years. Another independent distance measure can be derived from a timing parallax estimated in the global-fit timing solution. However, our measured timing parallax was found to be significantly covariant with an input DM parameter associated with free electrons from the solar wind. Such a covariance is unexpected since the solar-wind component of DM is strongest for pulsars close to the ecliptic plane, while PSR B1534+12 is  $\sim 30^\circ$  above the plane. Since the expected solar contribution is much smaller than the scatter of the 80-day DM bins in Figure

<sup>4</sup> <https://safe.nrao.edu/vlba/psrpi>

TABLE 4  
PROFILE-EVOLUTION MCMC PARAMETERS

Parameter	STA04 <sup>a</sup>	STA04	Mark IV	All
$\Omega_1^{\text{spin}}$ ( $^\circ/\text{yr}$ )	$0.44^{+4.6}_{-0.24}$	$0.51^{+0.15}_{-0.10}$	$0.48^{+0.10}_{-0.08}$	$0.59^{+0.10}_{-0.11}$
$\eta$ ( $^\circ$ )	$\pm 102^{+9}_{-9}$	$\pm 99^{+3}_{-4}$	$\pm 116^{+10}_{-23}$	$\pm 126^{+13}_{-23}$
$F'$	n/a	$-5.8^{+1.5}_{-1.4}$	$-2.7^{+1.5}_{-1.4}$	$-1.4^{+0.4}_{-0.7}$
$\epsilon$ ( $10^{-3}$ )	$1.5^{+0.6}_{-0.7}$	$-1.9^{+0.1}_{-0.1}$	$-1.2^{+0.1}_{-0.1}$	$6.7^{+0.1}_{-0.1}$

NOTE. — Uncertainties reflect 95% confidence intervals of posterior distributions.

<sup>a</sup> Original, non-MCMC results from STA04.

2, we chose to set the solar DM component to zero for the global timing fit while acknowledging that the timing parallax is unreliable as a fitted parameter.

#### 5.4. Precession and Geometry

Results from the MCMC fit on several data sets can be found in Table 4, and the posterior distributions for  $\Omega_1^{\text{spin}}$  derived from these sets are shown in Figure 5. We provided the original results obtained by STA04, as well as a reproduced set of results from the STA04 data set using the MCMC algorithm, for comparison with our extended Mark IV and ASP profiles. We assumed that values of  $F'$  must be negative while using the MCMC algorithm, since the simultaneous-linear-fit technique used and described by STA04, which avoids any consideration of  $F'$ , estimates that  $\cos \eta < 0$ . These results agree well with predictions from general relativity, where  $\Omega_1^{\text{spin}} = 0.51^\circ/\text{yr}$  using the derived masses in Table 3, and previous measurements made by STA04. General improvements in precision come from the new fitting procedure, which permitted direct sampling of the precession rate and other free parameters, as well as the addition of the ASP 2005 campaign and several strong bi-monthly observations.

The RVM analysis yielded values of  $\alpha$  and  $\beta$  at different times using the Mark III (reticon), Mark IV and ASP campaign profiles. The values of  $\beta$  measured for each campaign are shown in Figure 6. Measurements of  $\alpha = 103.5(3)^\circ$  are consistent with no evolution in time, while the values of  $\beta$  are found to change significantly, where  $d\beta/dt = -0.23 \pm 0.02^\circ/\text{yr}$ . This is consistent with the STA04 result of  $-0.21 \pm 0.03^\circ/\text{yr}$ . The assumption that general relativity is correct requires that  $d\beta/dt = \Omega_1^{\text{spin}} \sin i \cos \eta$ , and therefore yields  $\eta = \pm 117 \pm 3^\circ$  (68% confidence), which agrees with the value determined from the MCMC analysis described above. With these values, the misalignment angle  $\delta$  between the spin and orbital angular momentum axes can be derived through spherical trigonometry by  $\cos \delta = -\sin i \sin \lambda \sin \eta + \cos \lambda \cos i$ . The sign ambiguity in  $\eta$  and  $i$ , as well as the requirement that  $\cos i \tan \eta > 0$  pointed out by STA04, gives an expected value of  $\delta = 27.0 \pm 3.0^\circ$  or  $\delta = 153.0 \pm 3.0^\circ$ . Physical arguments based on alignment of angular momenta prior to the second supernova suggest that the smaller angle is correct (Bailes 1988), and therefore requires that  $\eta = -117 \pm 3^\circ$  and  $i = 77.7 \pm 0.9^\circ$ .

The consistency between the MCMC and RVM analyses serves as an improved, independent check of preces-

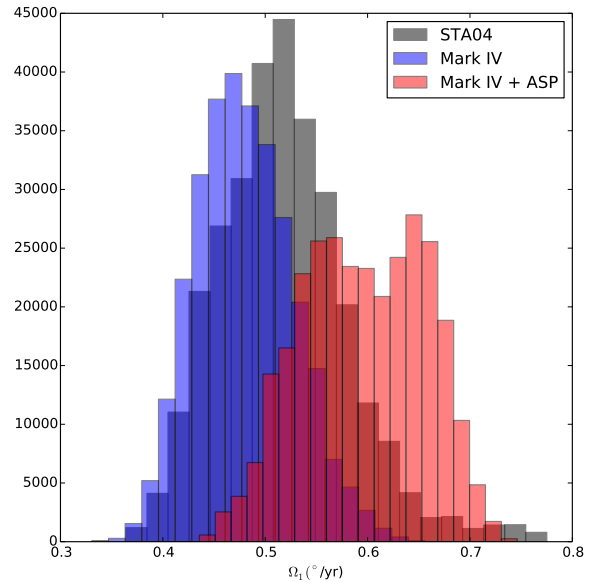


FIG. 5.— MCMC posterior distributions of  $\Omega_1^{\text{spin}}$  from the profile-shape analysis (see Section 5.4 for discussion). 300,000 samples were taken during the MCMC fit.

sion within this relativistic binary system. These results also confirm the geometric picture of this pulsar-binary system derived in STA04.

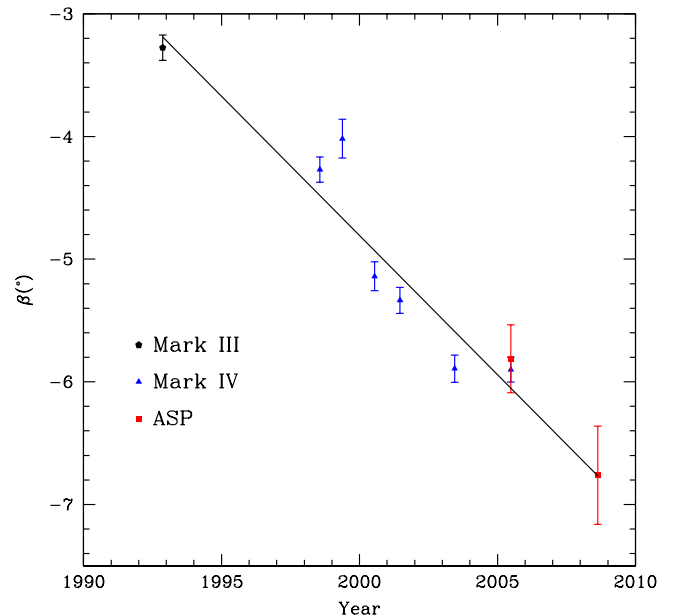


FIG. 6.— Impact angle  $\beta$  between the magnetic axis and line of sight as a function of time. The black line is a best-fit slope of  $-0.23 \pm 0.02^\circ/\text{yr}$ .

Konacki et al. (2003) pointed out that relativistic spin precession can eventually imprint a timing signature as a second-derivative in spin frequency. However, they predicted that it would take an additional 25 years of timing



observations in order to measure the predicted signature with reasonable accuracy. Moreover, our best-fit timing model of PSR B1534+12 data indicates that the measured  $\ddot{\nu}$  and  $\ddot{\nu}$  are dominated by timing noise.

### 5.5. Tests of General Relativity

In general relativity, each PK parameter is expressed as a function of at least one of the two binary-component masses; one can therefore define a “mass-mass” space where each PK parameter corresponds to a curve in this plane. Stairs et al. (1998) presented the first mass-mass plot that incorporated up to 5 PK curves, as well as the first “non-mixed” test of quasi-static parameters using the  $\dot{\omega} - \gamma - s$  combination.

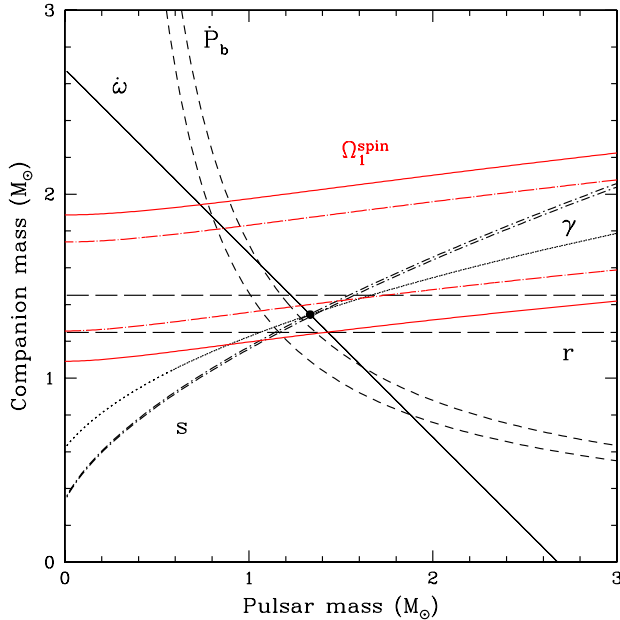


FIG. 7.— Mass-mass plot for PSR B1534+12. Each set of black curves represents the 68%-confidence region delimited by the labeled PK (timing) parameter. The dot-dashed and solid red curves represent the 68% and 95% confidence region determined from the spin-precession rate, respectively.

Figure 7 presents our evaluation of PK parameters and tests of general relativity using PSR B1534+12. Each curve corresponds to a PK value measured either with the best-fit DD timing model or profile-shape model, while the filled circle represents the best-fit DDGR solution of the pulsar and companion masses of  $m_1 =$

$1.3330 M_\odot$ ,  $m_2 = 1.3455 M_\odot$ , respectively. The  $\dot{P}_b$  curve was corrected for kinematic bias assuming a pulsar distance of  $d = 0.7 \pm 0.2$  kpc, which was estimated using the electron number-density model developed by Taylor & Cordes (1993), as discussed in Section 5.3. The discrepancy between this distance and the expected distance (Equation 4) prevents the curve from intersecting the other PK curves, while its large uncertainty dominates the corrected orbital-decay error estimate. The  $\Omega_1^{\text{spin}}$  curves intersect the best-fit DDGR point well at the 95% confidence level.

The Shapiro  $r$  parameter remains a slightly weaker constraint than the PK timing parameters, but its relative uncertainty has improved by nearly a factor of two since the last measurement by Stairs et al. (2002). The  $\dot{\omega} - \gamma - s$  combination is the strongest test from this pulsar and confirms general relativity to within 0.34% of its predictions. This test quality is slightly larger than the 0.05% test from the double-pulsar system, which uses the mass ratio as determined by the projected semi-major axes of both pulsars (Kramer et al. 2006).

The high-precision DDGR masses of PSR B1534+12 and its companion are consistent with previous estimates. As noted in Stairs et al. (2002), the significant difference between  $m_1$  and  $m_2$  presents a conundrum where the spun-up pulsar is actually less massive than its companion. This suggests that a period of “mass inversion” – mass transfer from the pulsar’s progenitor to its companion – took place during the system’s evolution, though a more thorough understanding of mass-transfer processes and its effects on stellar structure is needed. The effectiveness of mass estimates from Shapiro-delay measurements will continue to provide a better view of the general pulsar-companion mass population (Kiziltan et al. 2013).

The Arecibo Observatory is operated by SRI International under a cooperative agreement with the National Science Foundation (AST-1100968), and in alliance with Ana G. Méndez-Universidad Metropolitana, and the Universities Space Research Association. Pulsar research at UBC is supported by an NSERC Discovery Grant. We thank Z. Arzoumanian, F. Camilo, A. Lyne, D. Nice, J. H. Taylor, and A. Wolszczan for their earlier contributions to this project. We also thank P. Freire, I. Hoffman, A. Lommen, D. Lorimer, D. Nice, E. Splaver, and K. Xilouris for previous assistance with Mark-IV observations. We also thank R. Ferdman, M. Gonzalez, other NANOGrav observers for help with some of the ASP observations reported here.

### REFERENCES

- Antoniadis, J., Freire, P. C. C., Wex, N., Tauris, T. M., Lynch, R. S., van Kerkwijk, M. H., Kramer, M., Bassa, C., Dhillon, V. S., Driebe, T., Hessels, J. W. T., Kaspi, V. M., Kondratiev, V. I., Langer, N., Marsh, T. R., McLaughlin, M. A., Pennucci, T. T., Ransom, S. M., Stairs, I. H., van Leeuwen, J., Verbiest, J. P. W., & Whelan, D. G. 2013, *Science*, 340
- Arzoumanian, Z. 1995, PhD thesis, Princeton University
- Bailes, M. 1988, *A&A*, 202, 109
- Bell, J. F. & Bailes, M. 1996, *ApJ*, 456, L33
- Breton, R. P., Kaspi, V. M., Kramer, M., McLaughlin, M. A., Lyutikov, M., Ransom, S. R., Stairs, I. H., Ferdman, R. D., & Camilo, F. 2008, *Science*
- Burgay, M., D’Amico, N., Possenti, A., Manchester, R. N., Lyne, A. G., Joshi, B. C., McLaughlin, M. A., Kramer, M., Sarkissian, J. M., Camilo, F., Kalogera, V., Kim, C., & Lorimer, D. R. 2003, *Nature*, 426, 531
- Damour, T. & Deruelle, N. 1985, *Ann. Inst. H. Poincaré (Physique Théorique)*, 43, 107
- . 1986, *Ann. Inst. H. Poincaré (Physique Théorique)*, 44, 263
- Damour, T. & Taylor, J. H. 1992, *Phys. Rev. D*, 45, 1840
- de Sitter, W. 1916, *MNRAS*, 77, 155
- Demorest, P. B. 2007, PhD thesis, University of California, Berkeley



- Fonseca, E. 2012, Master's thesis, The University of British Columbia, <https://circle.ubc.ca/handle/2429/43498>
- Hankins, T. H. & Rickett, B. J. 1975, in *Methods in Computational Physics Volume 14 — Radio Astronomy* (New York: Academic Press), 55
- Hulse, R. A. & Taylor, J. H. 1975, *ApJ*, 195, L51
- Keith, M. J., Coles, W., Shannon, R. M., Hobbs, G. B., Manchester, R. N., Bailes, M., Bhat, N. D. R., Burke-Spolaor, S., Champion, D. J., Chaudhary, A., Hotan, A. W., Khoo, J., Kocz, J., Osłowski, S., Ravi, V., Reynolds, J. E., Sarkissian, J., van Straten, W., & Yardley, D. R. B. 2013, *MNRAS*, 429, 2161
- Kiziltan, B., Kottas, A., De Yoreo, M., & Thorsett, S. E. 2013, *ApJ*, 778, 66
- Konacki, M., Wolszczan, A., & Stairs, I. H. 2003, *ApJ*, 589, 495
- Kramer, M. 1998, *ApJ*, 509, 856
- Kramer, M., Stairs, I. H., Manchester, R. N., McLaughlin, M. A., Lyne, A. G., Ferdman, R. D., Burgay, M., Lorimer, D. R., Possenti, A., D'Amico, N., Sarkissian, J. M., Hobbs, G. B., Reynolds, J. E., Freire, P. C. C., & Camilo, F. 2006, *Science*, 314, 97
- Kuijken, K. & Gilmore, G. 1989, *MNRAS*, 239, 571
- Lorimer, D. R. & Kramer, M. 2005, *Handbook of Pulsar Astronomy* (Cambridge University Press)
- Nice, D. J. & Taylor, J. H. 1995, *ApJ*, 441, 429
- Radhakrishnan, V. & Cooke, D. J. 1969, *Astrophys. Lett.*, 3, 225
- Reid, M. J., Menten, K. M., Brunthaler, A., Zheng, X. W., Dame, T. M., Xu, Y., Wu, Y., Zhang, B., Sanna, A., Sato, M., Hachisuka, K., Choi, Y. K., Immer, K., Moscadelli, L., Rygl, K. L. J., & Bartkiewicz, A. 2014, *ArXiv e-prints*
- Shannon, R. M. & Cordes, J. M. 2012, *apj*, 761, 64
- Stairs, I. H., Arzoumanian, Z., Camilo, F., Lyne, A. G., Nice, D. J., Taylor, J. H., Thorsett, S. E., & Wolszczan, A. 1998, *ApJ*, 505, 352
- Stairs, I. H., Splaver, E. M., Thorsett, S. E., Nice, D. J., & Taylor, J. H. 2000, *MNRAS*, 314, 459, (astro-ph/9912272)
- Stairs, I. H., Thorsett, S. E., & Arzoumanian, Z. 2004, *Phys. Rev. Lett.*, 93, 141101
- Stairs, I. H., Thorsett, S. E., Taylor, J. H., & Wolszczan, A. 2002, *ApJ*, 581, 501
- Stinebring, D. R., Kaspi, V. M., Nice, D. J., Ryba, M. F., Taylor, J. H., Thorsett, S. E., & Hankins, T. H. 1992, *Rev. Sci. Instrum.*, 63, 3551
- Taylor, J. H. 1992, *Philos. Trans. Roy. Soc. London A*, 341, 117
- Taylor, J. H. & Cordes, J. M. 1993, *ApJ*, 411, 674
- Taylor, J. H., Wolszczan, A., Damour, T., & Weisberg, J. M. 1992, *Nature*, 355, 132
- Verbiest, J. P. W., Bailes, M., van Straten, W., Hobbs, G. B., Edwards, R. T., Manchester, R. N., Bhat, N. D. R., Sarkissian, J. M., Jacoby, B. A., & Kulkarni, S. R. 2008, *ApJ*, 679, 675
- Weisberg, J. M., Nice, D. J., & Taylor, J. H. 2010, *ApJ*, 722, 1030
- Wolszczan, A. 1991, *Nature*, 350, 688
- You, X. P., Hobbs, G., Coles, W. A., Manchester, R. N., Edwards, R., Bailes, M., Sarkissian, J., Verbiest, J. P. W., van Straten, W., Hotan, A., Ord, S., Jenet, F., Bhat, N. D. R., & Teoh, A. 2007, *MNRAS*, 378, 493